Journal Pre-proofs

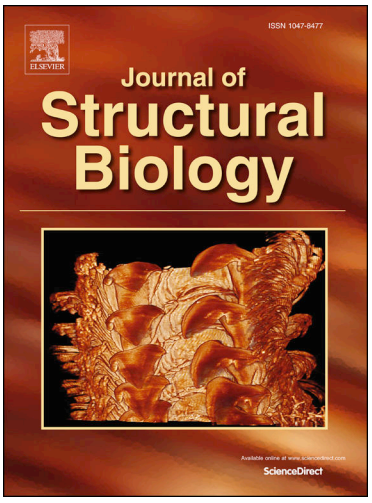

Research Article

Different strategies towards strength: Unveiling the role of Zn vs Mn/Ca and chitin arrangement in scorpion stingers

C. Sakr, P. Cook, M. Seiter, C. Hörweg, S. Ž ák, M. Cordill, M. Burghammer, M. Sztucki, H. Lichtenegger

PII: S1047-8477(25)00009-7
DOI: https://doi.org/10.1016/j.jsb.2025.108174
Reference: YJSBI 108174

To appear in: *Journal of Structural Biology*

Received Date: 18 June 2024
Revised Date: 16 January 2025
Accepted Date: 28 January 2025

Please cite this article as: Sakr, C., Cook, P., Seiter, M., Hörweg, C., Ž ák, S., Cordill, M., Burghammer, M., Sztucki, M., Lichtenegger, H., Different strategies towards strength: Unveiling the role of Zn vs Mn/Ca and chitin arrangement in scorpion stingers, *Journal of Structural Biology* (2025), doi: https://doi.org/10.1016/j.jsb.2025.108174

Different strategies towards strength: unveiling the role of Zn vs Mn/Ca and chitin arrangement in scorpion stingers.

C. Sakr[1,2], P. Cook[2,3], M. Seiter[4], C. Hörweg[4], S. Žák[5], M. Cordill[5], M. Burghammer[2], M. Sztucki[2], H. Lichtenegger[1]

1 BOKU University, Vienna, Austria

2 The European Synchrotron, ESRF, Grenoble, France

3 Danish Technological Institute, Taastrup, Denmark

4 Museum of Natural History, Vienna, Austria

5 Erich Schmid Institute of Materials Science, Leoben, Austria

- Distinct types of scorpions use different elemental distributions in their stingers.
- Chitin arrangement and elemental composition determine the mechanical properties.
- The presence of Zn is not always associated with hardening.
- Zn nanochannels were observed in stingers with epicuticle devoid of Zn.
- Mn/Ca incorporation increases epicuticle hardness and stiffness.

Synopsis

Examination of the role of different metal ions incorporation and the chitin structure in scorpion stingers gives better understanding on the enhancement of the specific biomechanical function of a biological material.

Keywords: Metal ions, chitin, scorpion stingers, mechanical properties.

Abstract:

Arthropods and especially scorpions often use metal ions to harden their cuticle. In this study we analyse the chitin fibre arrangement, metal content and distribution and mechanical properties of the stingers of two scorpions: the buthid scorpion *Centruroides platnicki* (PS) and the diplocentrid scorpion *Nebo whitei* (NS). Results show that both scorpions incorporate the same elements, Zn, Mn and Ca, but in different locations in the stinger cuticle. While NS uses Zn ions as hardening agent in the epicuticle, PS uses Mn/Ca ions. Interestingly, Zn ions were also found in PS but had no impact on the enhancement of the mechanical properties of the stinger. The use of different metal ions in biological materials is likely to enable precise adjustments of material properties to suit not only mechanical but biological functions as well.

I. Introduction

Arthropods have developed remarkable strategies to create hard body parts, such as stingers, fangs, and claws. These parts exhibit microscale variations in structure and composition, resulting in locally varying mechanical properties. The cuticle of arthropods, which forms their hard parts, consists of three main layers: a fibrous exocuticle and endocuticle which are made of chitin-protein fibrils [1-3] and a fibreless epicuticle based on sclerotised protein. Previous works have correlated the arrangement of the chitin fibrils in the cuticle of arthropods' hard parts with highly localised mechanical properties in the cuticle of arthropods [4-8].

However, the arrangement of chitin fibrils is not the only reinforcement strategy. It has been repeatedly shown that arthropods also use metal ions coordinated with the proteinaceous matrix, such as zinc (Zn), manganese (Mn), and calcium (Ca), for tailoring mechanical properties [9-21]. There is no deposition of mineralised crystals, in contrast to the deposition of calcium carbonates and phosphates observed in crustaceans [22], which also belong to the phylum of arthropods. In exceptional cases, small amounts of minerals have been found in insects, e.g. in the ovipositors of parasitic wasps [23]. Arthropods exhibit a fascinating variation in metal ion usage, even within the same organism. For instance, *Cupiennius salei* spiders have been shown to strengthen their fangs with Zn [15] and their claws with Mn and Ca [14]. This differential incorporation of elements results in different mechanical properties, with Zn associated with a higher modulus of elasticity

and the coexistence of Mn and Ca associated with greater hardness and wear resistance. In other cases, the incorporation of Zn has been correlated to higher hardness and wear resistance values [10]. Despite this evidence that metal ions enhance the mechanical properties of arthropod cuticle, the specific role of each element remains unclear.

Scorpions, in particular, have to produce high-performance material for their stingers that are used to penetrate their prey, including small vertebrates or the cuticle of other arthropods, even preying on their own siblings [24]. Previous studies of scorpion stingers have reported elevated levels of Zn and Mn, and the presence of the metal ions seemed to be correlated with greater hardness and stiffness locally [10]. Zn has been found mostly in the tip region and Mn detected mainly in the shaft [10, 11]. However, the exact location of these metal ions across the cuticle layers of the stinger was not differentiated in previous studies, as whole samples were examined. Additionally, the literature lacks differentiation between the role of metal ions in scorpion stingers and possible structural reasons for increased hardness and stiffness.

The present study focuses on scorpion stingers from two different species with distinct lifestyles: *Centruroides platnicki* (Armas, 1981; figure 1-A), belongs to the Buthidae family. It is distributed on the Lesser and Greater Antilles. In the tropical areas of the northern coast of the Dominican Republic, prey is abundant nearly year-round. This species is typically found on the ground and on bushes or trees. They experience conditions of extreme heat and high humidity throughout their lifetime. Their microhabitat is covered with many fallen leaves and small hiding places used to escape the daytime heat. During nighttime they are active hunters and rely heavily on using their stinger to capture prey. Their life cycle is completed in less than 10 months (M. Seiter, pers. comm.) excluding embryonic development.

Nebo whitei (Vachon, 1980; figure 1-B), belongs to the Diplocentridae family and occurs on the Arabian Peninsula. *N. whitei* is adapted to living in small cracks and underneath stones and is often found in desert environments on the southern part of Oman. In this region with seasonal rainy and 'hibernation' seasons, prey abundancy varies over the year. It is a typical sit-and-wait predator: they primarily catch their prey using their strong pedipalps, and rarely use their stinger to inject venom (M. Seiter, pers. comm.). *N. whitei* needs several years to reach adulthood and have an embryonic development time of about 8-10 months.

We found that both species incorporate Zn, Mn and Ca metal ions into their stinger cuticle but with different localisation, suggesting an adaptation for specific mechanical or biological functions.

To get a deeper understanding of this fascinating biological material, this work presents quantitative and qualitative information obtained by SEM, nano-resolved XRF and XRD, and nanoindentation analysis.

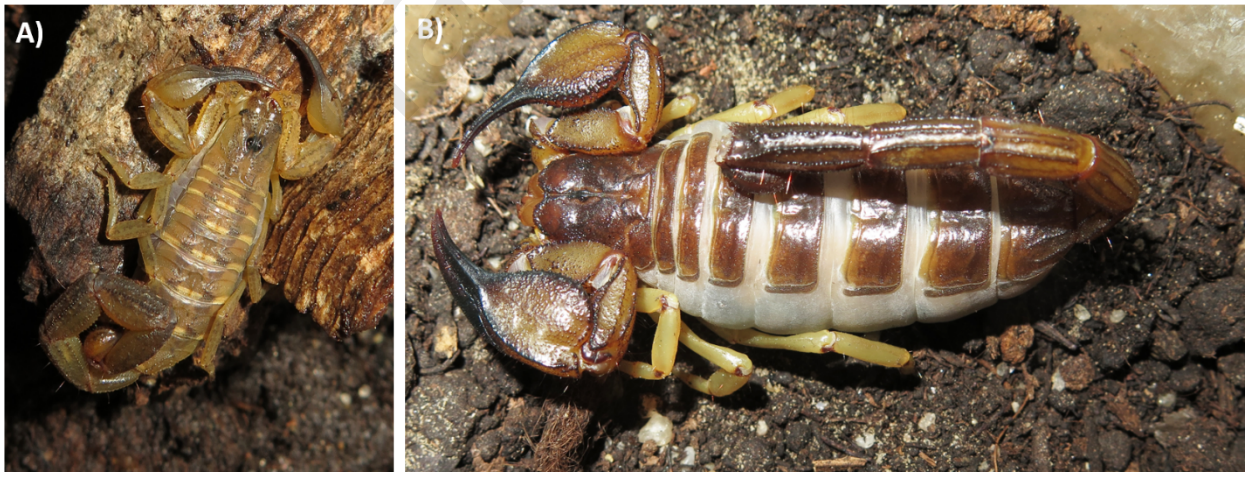

Figure 1 - Top view of A) *Centruroides platnicki* and B) *Nebo whitei*.

II. Experimental section

1) Scorpion stingers:

Stingers from *C. platnicki* (hereafter referred to as PS) and *N. whitei* (hereafter referred to as NS) were obtained from the collections of the Natural History Museum of Vienna, Austria.

C. platnicki scorpions were collected from Hato del Medio Arriba, Monte Cristi Prov., Dominican Republic @N19°41.584'; W71°18.2065'; 66m. *N. whitei* scorpions were collected in Southern Oman, north-western Taqa, Tobruk Oase @17°06'00.1"N 54°19'35.1"E.

9 PS and 6 NS samples from adult scorpions were used in this work.

2) Sample embedding and preparation:

Stingers with the venom bladder were first cut from dead scorpions and kept in an 80% ethanol solution at room temperature. After separating the stingers from the bladder, samples planned for embedding were completely dehydrated by using a 100% ethanol solution. After dehydration, the stingers without the venom bladder were embedded in Technovit 7100, a cold curing resin based on hydroxyethylmethacrylate (HEMA). Due to the dense, non-porous structure of the stingers, the resin did not fully infiltrate the sample tissue. Resin blocks were polymerised at room temperature. For synchrotron X-Ray Fluorescence (XRF) and X-Ray Diffraction (XRD), the embedded samples were sectioned with a tungsten carbide knife using an RMC Boeckeler MT-990 rotary microtome into 10 µm thick longitudinal and cross sections. The remaining blocks were polished and used for nanoindentation and SEM measurements. Whole stingers were also used for XRF measurements.

3) Scanning Electron Microscope (SEM) images:

SEM investigations were carried out at the Institute of Physics and Materials Science (IPM) in Vienna, Austria using FEI Quanta FEG 250 SEM and a Gaseous Secondary Electron Detector (GSED). Embedded and polished samples were used. The samples were then mounted on SEM specimen stubs and coated with a thin layer of gold to avoid surface charging.

4) X-Ray Diffraction (XRD) and X-Ray Fluorescence (XRF) mapping:

For an overview of the elemental composition of the stingers, XRF measurements were conducted on whole stingers as well as longitudinal sections at beamline BM05 at the European Synchrotron Radiation Facility (ESRF). An x-ray beam with the energy of 13 keV (λ = 0.953 Å) was focused to a 12x10 μm^2 spot using beryllium Compound Refractive Lenses (CRLs). XRF maps were obtained by scanning the samples in a raster pattern and data were collected using a Vortex EM Si drift diode detector. The exposure time was 1 s per scan point. For nano-resolved XRD and XRF maps, 10 µm thick longitudinal and cross sections placed on silicon nitride membranes (1 µm thick) were scanned at ESRF beamline ID13. The membranes were glued on the edge of a glass microscope slide and mounted on a piezo stage for nano-resolved movements. The beam energy was 15.2 keV (λ = 0.815 Å), and the beam was focused to 100x100 nm^2. The exposure time was 50 ms per scan point to avoid beam damage, which is particularly relevant for XRD. XRD maps were collected with an EIGER X 4M detector. XRF maps were collected using a single element Vortex EM Si drift diode detector placed downstream from the sample in transmission mode at an angle of ~105 degrees to the incident x-ray beam. For XRD, the sample-detector distance was calibrated using aluminium oxide (Al_2O_3) powder. The intensity in all the XRF and XRD maps was normalised with the storage ring current.

XRD data evaluation:

As a first step, the 2D diffraction patterns were azimuthally integrated using pyFAI [25] to obtain 1D curves of intensity versus the scattering vector q and versus the azimuthal angle χ, respectively. The scattering vector is defined as ($q = 4\pi \sin(\theta)/ \lambda$) with 2θ being the scattering angle and λ being the wavelength of the incident x-rays. All integrated data were normalised with the background. In order to get qualitative and quantitative information about the chitin fibrils, separate regions of interest were defined and XRD patterns averaged within this region to enhance the signal quality. To study the degree of crystallinity of the chitin in the stinger, we used the following equation:

$$\text{degree of crystallinity} = A_c / (A_c + A_a) \quad \text{(eq 1)}$$

where A_c is the area under the crystalline peaks and A_a is the area under the amorphous background.

XRF data evaluation:

The software pyMCA[26] was used to evaluate the XRF maps. After calibration, all elements present were identified in a summed XRF spectrum obtained from all scan points in one map. Peak fitting was performed using a batch process to generate the elemental maps.

For XRF, an AXO standard with several elements (Fe, Cu, Ti, Cr – reference number: RG01-200-S5461-43) deposited on silicon nitride membrane was measured for a semi-quantification of the concentration of the element present in the stingers. Our semi-quantification process was performed on the same samples that we performed nanoindentation on. Since those samples are composed of the remaining of the stingers embedded in HEMA blocks, a geometrical correction was necessary to get the thickness of the matrix that contains the metal ions. First, each area measured was considered as a cross section of a quarter of an ellipsoidal hollow cylinder (fig S1).

Then the average concentration is obtained over a line along the axis of the stinger in the measured area with the calculated thickness. (details can be found in the supplementary information I).

5) Nanoindentation:

The mechanical properties of the samples were probed using a TS77 Select Bruker-Hysitron nanoindentation platform available at the Erich Schmid Institute of Materials Science, Leoben, Austria and a new, well-calibrated cube-corner diamond tip. The area function and frame compliance calibrations were made using 100 quasi-static Open-Loop (OL) indents into fused silica for each calibration run with a 10 s load—5 s hold—10 s unloading profile and maximum loads between 50 μN and 10 mN, resulting in the calibrated area function for indentation depths between 10 and 500 nm.

In the regions of interest, a grid mapping of the mechanical properties was performed using rectangular grids of indents with the spacing between the indents set to 3 μm for NS and 2 μm for PS. The indents were displacement controlled and the maximum indentation depth was set to 400 nm, whereas the loading and unloading times were 5 s each with no hold time at the maximum load. The spacing of indents was selected to map the mechanical properties of mm-scale samples with high-enough resolution while ensuring no influence of the adjacent indents. According to Sudharshan Phani and Oliver [27], the indentation spacing depends on the indentation depth and the angle of the indenter tip – the spacing should be larger than 1.5-times of the indent contact lateral dimension. This condition is fully satisfied for the maximum indentation depth as well as resulting contact depths of indents (roughly around 300 nm). In total, 6 grids (maps) spanning the distance between 0 μm and 900 μm from the sample tip and consisting of 3747 indents on NS and 9 grids (maps) spanning the distance between 50 μm and 1400 μm from the sample tip and

consisting of 4770 indents on PS were made and analysed. Indented areas also cover a small portion of the embedding material to measure a reference value of material which is not the sample itself.

All of the resulting load–displacement curves were analysed using the standard Oliver and Pharr method [28] and the calibrated area function. The outputs of the nanoindentation are the hardness, H, and the reduced elastic modulus, E_r (elastic response of both the indenter and the indented sample), which is related to the actual elastic modulus of the sample according to this formula:

$$1/E_r = (1 - \nu_i^2)/E_i + (1 - \nu^2)/E$$

where E_i and ν_i are Young's modulus (1140 GPa) and Poisson's ratio (0.07), respectively, of the diamond indenter material and E and ν are Young's modulus and Poisson's ratio of the indented sample, respectively. However, since the Poisson's ratio of the samples is unknown, only the reduced elastic modulus E_r will be presented in this work.

III. Results:

1) Morphology:

Stinger morphology was studied by SEM. Fig. 2A shows the tip of a PS stinger with the openings of the venom canal placed at the dorsal part of the stinger. A fracture surface at the tip as well as a longitudinal section of the stinger show the venom canals, as well as the cuticle layers: the epicuticle marked with an orange cross and adjacent to it the exocuticle marked with a blue cross of the stinger (fig. 2B,D). A higher magnification shows the exocuticle's densely packed fibre sheets parallel to each other that are oriented roughly along the stinger and appears to be rotated around the stinger axis (fig. 2C). At the base of the stinger, the endocuticle, marked with a green cross, is present (fig. 2E). High magnification images of the endocuticle reveal a typical lamellar

Bouligand structure (fig. 2F) as reported in [29]. The exocuticle shows a gradient in thickness along the stinger. For instance, in fig 2-D the average thickness of the exocuticle is 21 µm while in fig 2-E the average thickness of the exocuticle is 46 µm.

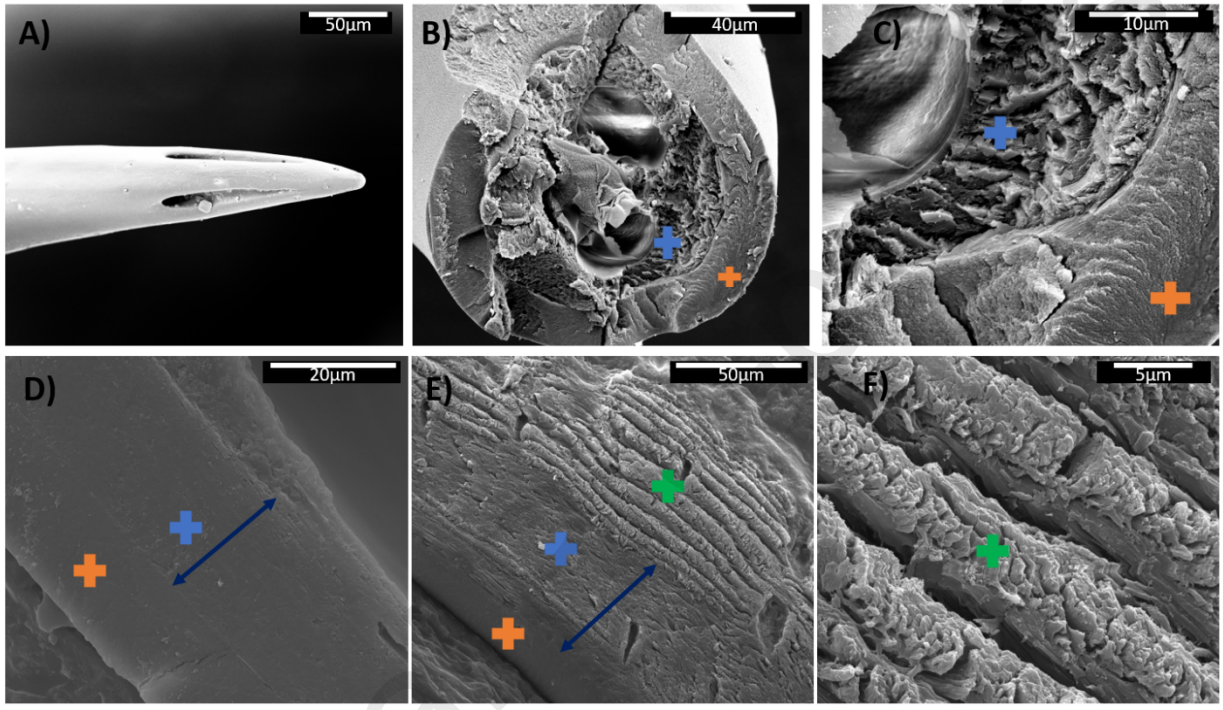

Figure 2: SEM images showing: A) the tip of PS. B) fracture surface of PS. C) High magnification image of the fracture surface showing the fibreless epicuticle (indicated with orange cross), the exocuticle where the chitin-protein fibrils sheets are rotated and arranged along the stinger axis and the venom canals (indicated with blue cross). D) longitudinal section close to the tip of PS showing the epicuticle (orange cross) and exocuticle (blue cross). Arrows indicate the total thickness of the exoculticle. E) longitudinal section at the base of PS showing in additional layer, i.e. the exocuticle. F) high magnification image of the base showing the endocuticle with the chitin-protein fibrils showing a Bouligand structure (indicated with green cross).

2) Chitin crystal structure in PS and NS:

Local XRD measurements across the length of the entire stinger reveal information on the crystalline chitin fibrils. Figure 3 shows the results acquired from different regions of PS. Area 1 denotes the position of the opening of the venom canal. Area 2, 3, 4 and 5 denote the selected

positions below the venom canals opening as showed in figure 3-A respectively (fig. 3A). Due to the high-resolution mapping (100 nm steps across the cuticle layers), we could differentiate the signal obtained from the epicuticle and exocuticle. The signal from the exocuticle readily shows the diffraction patterns of the chitin crystals (fig. 3A). In contrast, at the epicuticle, no chitin diffraction patterns were observed in the scanned areas along the stinger suggesting that the epicuticle does not contain chitin fibrils and it is only formed by proteinaceous tissue, also reported in other arthropods cuticle [15]. Similarly, at the very tip of the stinger no diffraction pattern was obtained. From the averaged diffraction patterns over the selected areas in the exocuticle (as shown in fig. 3A in black squares), XRD patterns reveal the preferred orientation of the chitin fibrils in the noted areas of the stinger, which is represented by white arrows. In order to study the degree of alignment of the chitin fibrils, the XRD signal was integrated over the azimuth and the FWHM of the integrated intensity of the (002) reflection was obtained by a Gaussian fit (fig. 3B.i). The values of the FWHM are represented in figure 3B.ii as a function of the distance from the opening of the venom canals. Close to the opening of the venom canals, i.e. area 1 and 2, the FWHM is between 6° and 10° and increases progressively to 15° at the base of the stinger (D = 1030 µm). This suggests that there is strong preferred orientation close to the tip of the stinger and the fibrils are oriented parallel to each other. The orientation becomes less pronounced at the base of the stinger This could also be seen in the diffraction pattern at area 5 where the diffracted intensity becomes continuous around the azimuthal angle (fig. 3A) with a maximum of intensity belonging to the oriented parallel chitin fibrils in the exocuticle.

From eq1, the degree of crystallinity of the chitin crystals was determined as well at different position in PS. At the venom canal opening the degree of crystallinity is about 12% and increases to 24.5% at the base of the stinger. Values of the degree of crystallinity in all measured regions are

presented in figure 3B.iv. The same study was done on a 10 µm longitudinal section obtained from the shaft of NS figure 3C. The FWHM and the degree of crystallinity in the measured areas are presented in figure 3D. Comparing to PS, NS shows lower values of the degree of crystallinity in the areas close to the base. In contrast, the FWHM was in the same range. Unfortunately, due to the lack of samples, only one section of NS could be studied and this section contained the shaft only, but not the stinger tip.

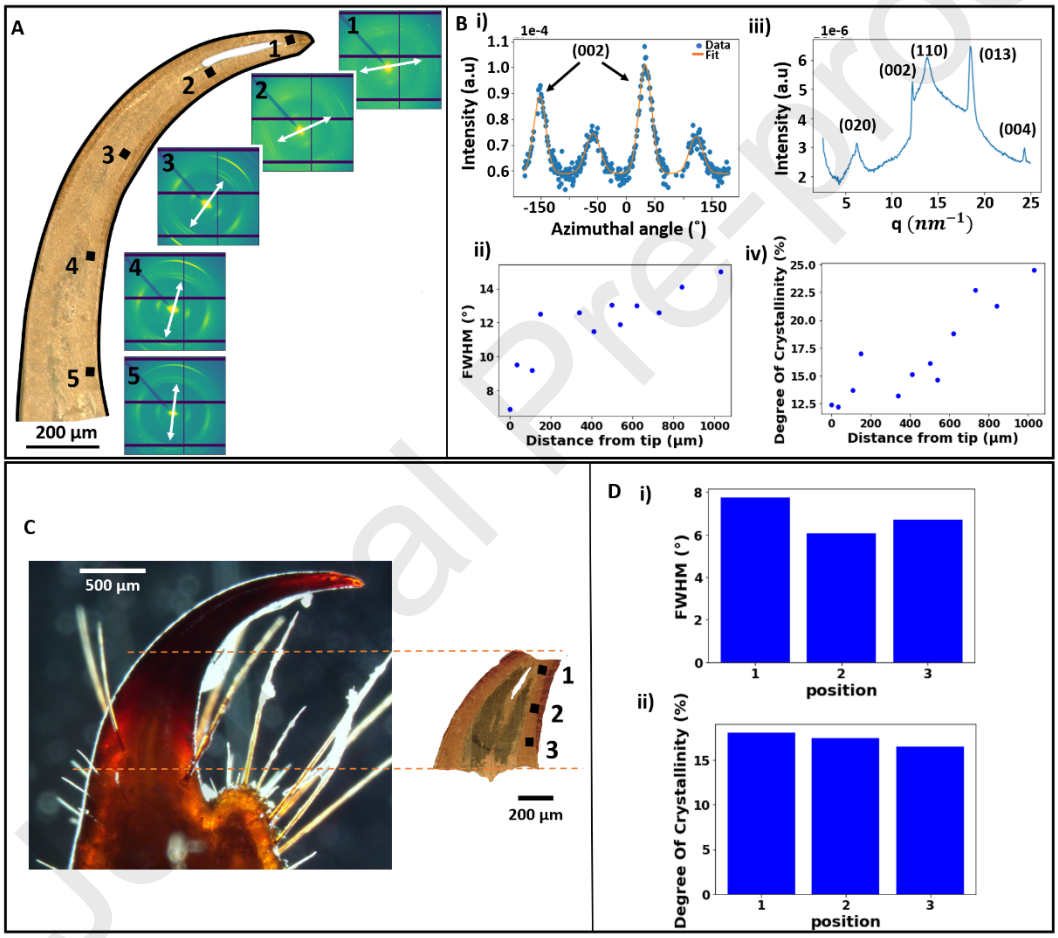

Figure 3: A) microscope image of a longitudinal section of PS with 2D diffraction images showing the orientation indicated with white arrows of the chitin fibrils in the exocuticle along PS. The diffraction patterns were obtained by averaging signal XRD patterns over the areas indicated with the black squares. B)i) Fitted profile of the intensity of the (002) reflection along the azimuthal angle. B)ii) Histogram showing the evolution of the FWHM of the (002) intensity along the azimuthal angle in the measured regions of PS B)iii) radial XRD intensity profile of the chitin. B)iv) histogram showing the evolution of the crystallinity of the chitin along the measured areas in PS. C) microscope

image of a whole NS and a longitudinal section of the shaft (indicated with two dashed yellow lines) of NS. D.i) Histogram showing the evolution of the FWHM of the (002) intensity along the azimuthal angle in the measured regions in NS. D.ii) histogram showing the evolution of the crystallinity of the chitin along the measured areas in NS.

3) Elemental composition

The elemental composition and distribution along both PS and NS were studied by X-Ray fluorescence (XRF). Results from low resolved XRF maps on whole stingers show the presence of different elements such as Zn, Mn and Ca (fig. 4A.i, ii). Other trace elements like Ar, Cl, S, Ni and Cu were also found (fig. 4B.i, ii). It is already obvious from the images that the distribution of the elements in NS and PS differs considerably. NS shows a familiar distribution of the elements with Zn in the tip of the stinger and Mn and Ca in the shaft region of the stinger, which is found in many of arthropod hard parts and also in scorpion stingers [10, 11]. By contrast PS shows a peculiar distribution of Zn, Mn and Ca, with Mn and Ca in the tip region and the shaft and Zn only present in the inner part of the stinger.

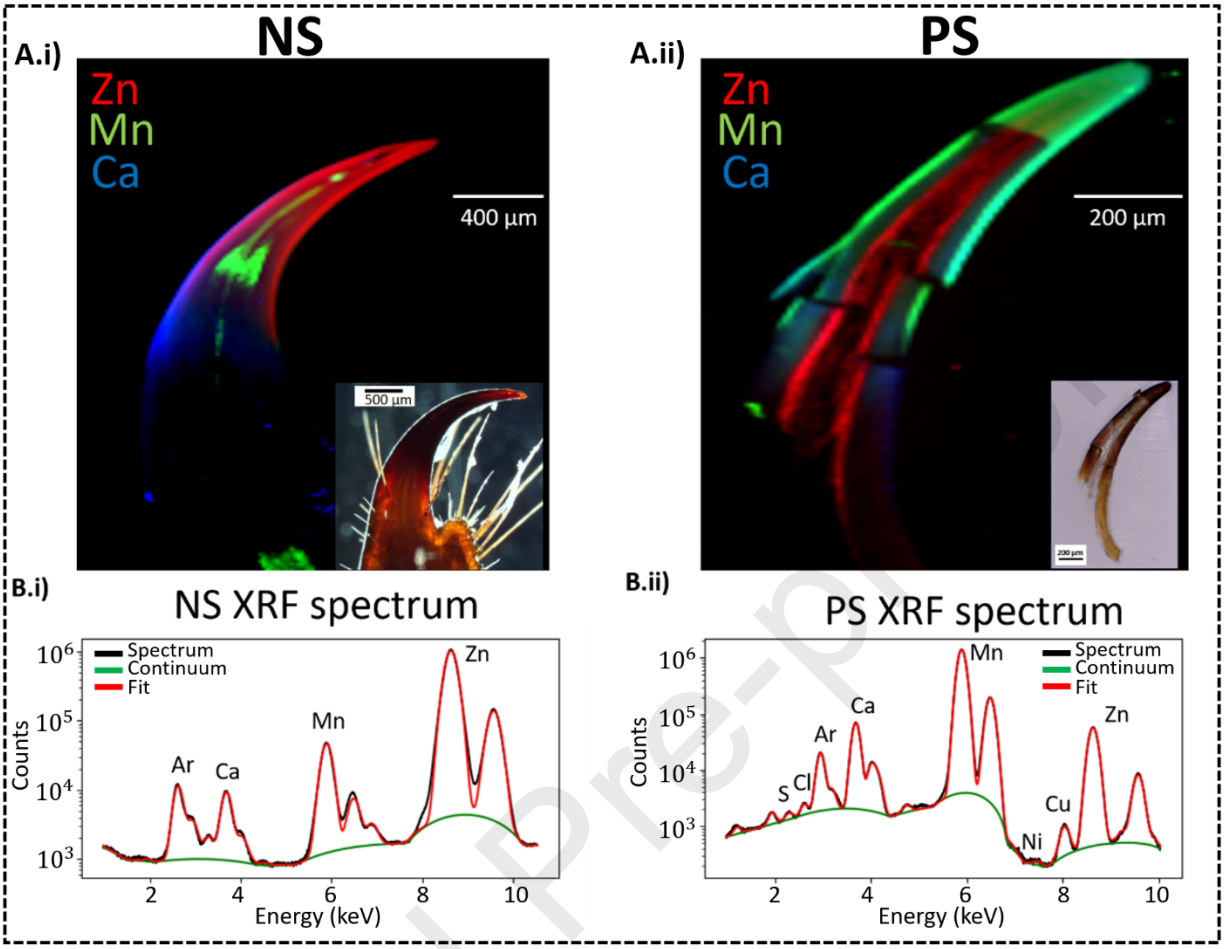

Figure 4: low resolution XRF maps showing the distribution of Zn, Mn and Ca in: A.i) whole NS , A.ii) sectioned PS. B.i) and B.ii) show the XRF spectrum of NS and PS respectively.

Nano-resolved XRF maps from the whole tip, longitudinal and cross-section of PS reveal better insight on the localisation of the elements in the cuticle layers. We found that Zn is located in nanometric stripes oriented vertically along the stinger that end up around the venom canal opening (fig. 5A.i, B.i, ii, iii) and some of them pass through the epicuticle. In addition, Zn is also found in a thin line forming an interface between the epicuticle and the endocuticle (fig. 5B.v) as well as in the venom canals wall in high concentration (compared to the amount of Zn found in the nano stripes). However, Mn and Ca co-exist in the epicuticle of the stinger.

Figure 5C.i shows high resolved XRF maps at the shaft of NS where we found Zn in the epicuticle in high quantity and Mn and Ca in low quantities only at the surface of the epicuticle.

Semi-quantitative XRF analysis was done on the same stingers used for nanoindentation in order to correlate the incorporation of the metal ions with the mechanical properties later on (see supp information). As described in the methods section, semi-quantitative analysis was carried out and a geometrical correction was done on the local thickness of the epicuticle for both PS and NS (XRF concentration maps are shown in fig S2 in supplementary information I). After correction with the absorption of the matrix (here considered as chitin only with density of 1.425g/cm^3) and the embedding material (HEMA with density of 1.07g/cm^3), we found that the concentration of Mn/Ca in PS is maximum with a value of 0.88/0.33 wt% close to the tip and decreases gradually along the stinger axis and shows a minimum of 0.063/0.13 wt% near the base. At the base, the epicuticle is free of metal ions. For NS the concentration of Zn is 0.94 wt% close to the tip and decreases to 0.058 wt% near the base. In contrast, the concentration of Mn/Ca increases from 0.07/0.09 wt% close to the tip to 0.15/0.7 wt% close to middle of the stinger. At the base, the epicuticle is free from metal ions. Concentration of Zn, Mn and Ca in the other measured regions along PS and NS are shown in table 1.

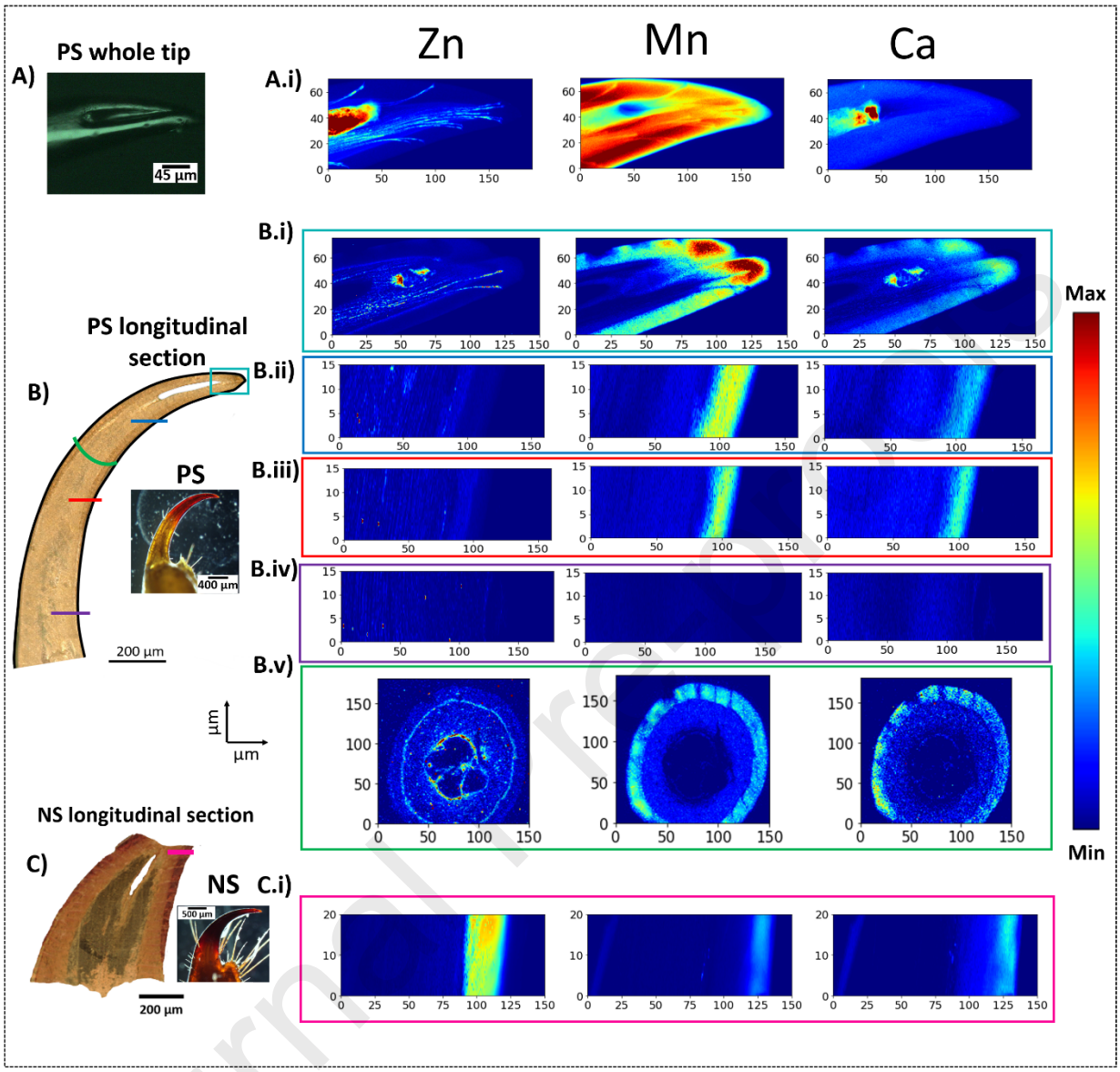

Figure 5: A) light microscopy image of PS whole stinger. A.i) nano-resolved XRF maps showing the distribution of Zn, Mn and Ca in the whole PS tip. B) light microscope image of a PS longitudinal section and whole PS. B.i, ii, iii, iv) nano-resolved XRF maps showing the distribution on Zn, Mn and Ca in the indicated areas in the longitudinal section in B). B.v) nano-resolved XRF maps showing the distribution on Zn, Mn and Ca in a cross section in the middle part of PS. The scale of the nano-resolved XRF maps is indicated in µm. C) light microscope image of a NS longitudinal section at the shaft and whole NS. C.i) nano-resolved XRF maps showing the distribution of Zn, Mn and Ca in the highlighted area in pink. All XRF maps are scaled in µm.

4) Mechanical properties:

Nanoindentation measurements were performed on the epicuticle and the exocuticle in various locations on both PS and NS in dry conditions to study the local variations of the mechanical properties in the cuticle layers.

Results from each indentation, comprised of the hardness, H, and reduced elastic modulus, E_r, were also complemented by their coordinates within the indentation grid. In combination with confocal laser scanning microscopy (CLSM) imaging after the indentation, each map could be overlaid on the longitudinal section image of the stinger (fig. 6). Note that the indentation grids at the very tip of NS were not used. Due to the separation of the sample from the embedding resin in this area, a cavity was formed under the tip of the stinger. This cavity caused the poorly supported stinger to behave like a spring, resulting in material properties lower than for the embedding resin. Therefore, these maps were excluded from the evaluation.

A consistent value for the resin confirms no variation in embedding material and rules out any systematic error which could happen during individual mapping. Furthermore, due to the dense, non-porous structure of the stingers, the resin did not fully infiltrate the sample thus we are confident that it did not affect the indentation results

For PS, in the epicuticle, where Mn and Ca co-exist, the mean value of the reduced elastic modulus E_r and the Hardness H are maximum with a value of 10.17± 0.24 GPa and 0.68± 0.03 GPa respectively, at the tip where Mn and Ca co-exist in high concentrations and decrease to E_r = 5.26 ± 0.15 GPa and H = 0.37 ± 0.03 GPa respectively, at the base which is free from the metal ions.

In the exocuticle, the values of E_r and H along the stinger are constant and are about 8.26 ± 0.24 GPa and 0.49 ± 0.03 GPa on average respectively.

For NS, in the epicuticle, where Zn is incorporated, the value of the reduced elastic modulus E_r is 10.14 ± 0.84 GPa and the Hardness H is 0.71 ± 0.04 GPa. Both, Er and H decrease towards the base in parallel with a decreasing Zn content. In the exocuticle, the values of E_r and H are about 7.30± 0.75 GPa and 0.46 ± 0.34 GPa on average, respectively. Values of hardness H and reduced elastic modulus Er in all indented regions are shown in table 1.

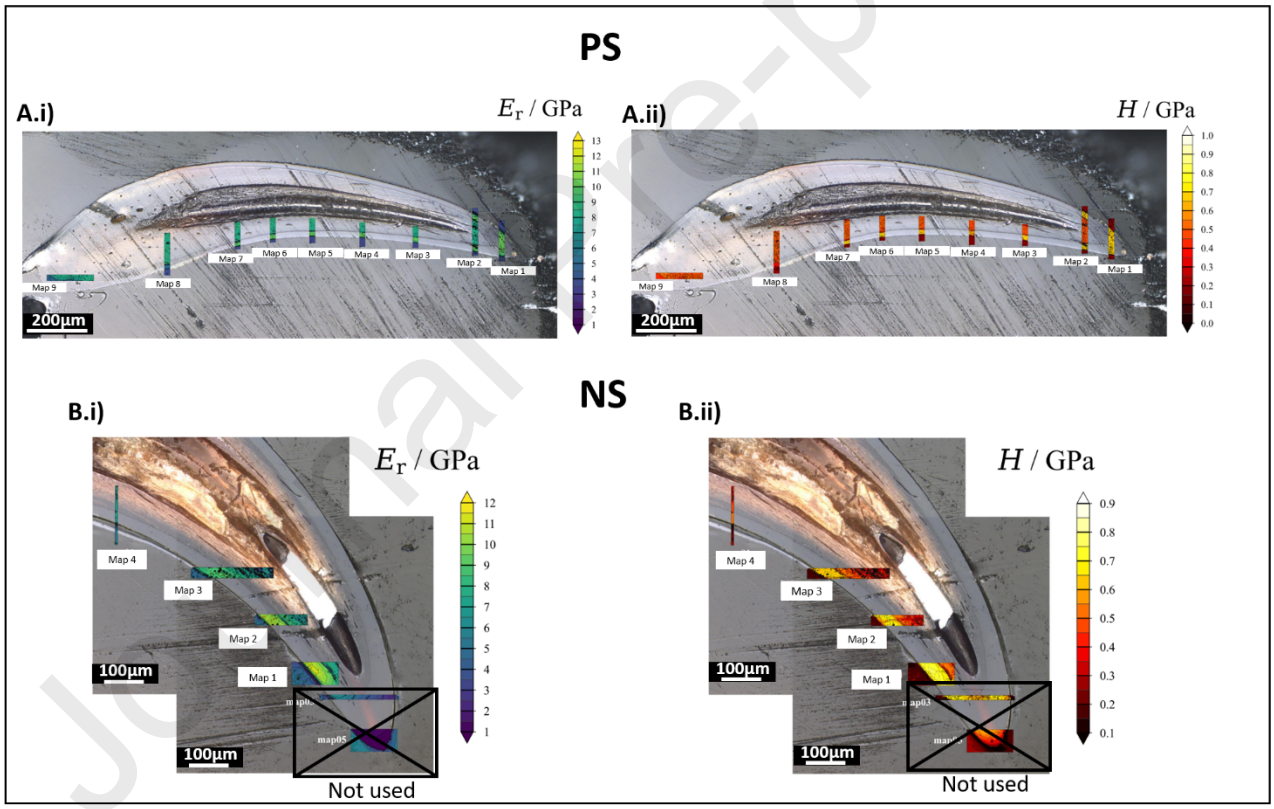

Figure 6: Overview results of the reduced elastic modulus in A.i) PS and B.i) NS and hardness is A.ii) PS and B.ii) NS. The crossed areas in NS were not taken into consideration.

Table 1: Resulting hardness and reduced elastic modulus of the epicuticle and exocuticle for both and the concentration of Zn, Mn and Ca found in the epicuticle of PS and NS in the measured areas

PS							
Maps	Epicuticle		Exocuticle		Concentration (Epicuticle) ±0.1wt%		
	H / GPa	Er / GPa	H / GPa	Er / GPa	Zn	Mn	Ca
Map 1	0.68 ± 0.03	10.17 ± 0.24	---	---	---	0.88	0.30
Map 2	0.67 ± 0.04	9.96 ± 0.29	0.49 ± 0.02	8.08 ± 0.18	---	0.87	0.29
Map 3	0.66 ± 0.02	9.99 ± 0.19	0.49 ± 0.02	8.13 ± 0.15	---	0.79	0.38
Map 4	0.63 ± 0.03	9.97 ± 0.28	0.48 ± 0.03	8.18 ± 0.22	---	0.73	0.32
Map 5	0.63 ± 0.03	9.92 ± 0.27	0.49 ± 0.03	8.33 ± 0.29	---	0.65	0.35
Map 6	0.69 ± 0.03	10.06 ± 0.23	0.5 ± 0.04	8.46 ± 0.32	---	0.60	0.29
Map 7	0.66 ± 0.04	9.8 ± 0.25	0.49 ± 0.03	8.32 ± 0.29	---	0.53	0.26
Map 8	0.37 ± 0.03	5.26 ± 0.15	0.49 ± 0.03	8.38 ± 0.27	---	0.063	0.13
NS							
Maps	Epicuticle		Exocuticle		Concentration (Epicuticle) ±0.1wt%		
	H / GPa	Er / GPa	H / GPa	Er / GPa	Zn	Mn	Ca
Map 1	0.71 ± 0.04	10.14 ± 0.84	0.51 ± 0.02	7.45 ± 0.31	0.94	0.11	0.078
Map 2	0.68 ± 0.03	10.3 ± 0.31	0.47 ± 0.12	7.81 ± 1.24	1.1	0.26	0.22
Map 3	0.63 ± 0.02	8.81 ± 0.32	0.44 ± 0.14	7.36 ± 1.16	0.50	0.57	0.56
Map 4	0.54 ± 0.01	7.03 ± 0.27	0.44 ± 0.08	6.6 ± 0.32	0.058	0.57	0.86

IV. Discussion:

For predation and defence, a substantial number of scorpions rely on their sharp stingers to inject venom, subjecting these stingers to extreme mechanical loads. Here we discuss the correlation of metal ions incorporation with the mechanical properties of the scorpion stinger and discuss potential drivers for its development.

As shown in Figure 2, the PS cuticle comprises three layers, consistent with findings in the literature: the epicuticle is the outermost layer of the cuticle, which is formed by a cross-linked protein matrix [15]. Adjacent to it, we find the exocuticle which is only present beneath the venom canal opening and it is not present at the very tip of the stinger. It is characterised by chitin fibres wrapped in protein matrix which are arranged parallel to each other along the stinger. This unique arrangement of the chitin fibrils provides the stinger a high axial stiffness to resist applied axial forces and bending moments but a low shear stiffness and low resistance the twisting moments [30]. The third layer is the endocuticle which is formed by chitin fibres arranged in Bouligand structure and it is only found at the base of the stinger. The Bouligand structure found in most of arthropods cuticle, (e.g. fangs [15] or claws [31, 32]) provide a high shear stiffness [30]. The shear stiffness has been shown to be between five and two orders of magnitude greater than that of the parallel fibres array, which resists the twisting moments [30]. From a mechanical functional point of view, when the stinger enters the prey's cuticle, it might face bending and torsion stresses since the prey can start moving in any direction before it gets paralysed by the scorpion venom. Therefore, chitin fibrils in parallel and Bouligand arrangement could be seen as a structural adaptation designed to resist bending and torsion stresses, respectively.

The epicuticle layer is the first part of the stinger that faces high mechanical loads while stinging. Like other arthropods, the epicuticle layer of scorpion stinger is made of protein matrix crosslinked with metal ions. The most common metal ion used as hardening agent is Zn [10, 12, 15]. Zn at elevated levels is also found in the epicuticle of NS, with higher Zn content closer to the tip region. However, in the PS, only Mn and Ca metal ions are found in the epicuticle. Zn is found in the exocuticle in nanochannels, around the venom canals and in a thin layer separating the epicuticle from the exocuticle (figure 4- B.i, C.v). It has been postulated in the literature that nanochannels found in arthropods hard parts are used to transport Zn ions after ecdysis for protein cross-linking in high concentrations [13, 33]. While in NS, Zn channels are associated with a Zn rich epicuticle, our findings in PS oppose these observations since only Mn and Ca are incorporated in the epicuticle in high concentration. It is important to note that all of the studied stingers come from adult scorpions, ruling out the possibility of the incorporation of Zn in the epicuticle in later stages of hardening. Therefore, Zn metal ions in this case should have other functionalities. The observed highly-localised occurrence of Zn in the layer covering the venom canal (fig 4- B.i, C.v) could point to additional or different functionalities than just mechanical support. In a biologically remote but functionally similar context, it has been suggested that metal ions in the teeth of a poisonous worm could be used for enzymatic activation of the venom [34]. We speculate that the location of Zn close to the venom canal in PS could be related to the fact that many scorpions produce venom with Zn containing metalloproteases [35] . This may also explain the high Zn levels apparent in the venom canal (see Fig. 4 B i). While the function of the Zn layer at the epicuticle-exocuticle interface remains unclear, we hypothesise that its incorporation may contribute to the stabilisation of the exoskeleton's hierarchical structure, enhancing mechanical properties and providing additional support at stress-concentrating junctions. Additionally, Zn is a

well-known antimicrobial agent, and its presence in the exoskeleton could serve as a defence mechanism, helping to protect against microbial colonisation and preventing external infections [36].

The incorporation of only Mn and Ca in the stinger reveal additional insights on the strategy of hardening stinging tools. It has been shown that Mn and Ca were also used as hardening agents in the *C. salei* spider claws and resulted in high values of wear resistance and hardness [14]. In contrast, in the termite *Coptotermes acinaciformis* Mn was found but had no impact on any mechanical properties [20]. Mn was also found in the stinger of the caraboctid scorpion *Hadrarus. arizonensis* but located in the shaft of the stinger and not in the tip, where Zn metal ions were found [10, 11]. In our study, nanoindentation measurements were conducted on both PS and NS to gain a better understanding of the influence of Zn, Mn, and Ca on the mechanical responses of the stingers. Comparing the mechanical properties of regions close to the tip (the very tip of both stingers was not indented due to experimental difficulties, see previous chapter) provides insight into possible biomechanical adaptation. Figure 7 illustrates the reduced elastic modulus E_r, Hardness H, as a function of the concentration of Mn, Ca in PS and Zn in NS. In the case of NS, the E_r and H depend on the concentration of Zn and they decrease linearly as the concentration of Zn decreases, which is in agreement with results in the literature [12, 15]. In PS we observe that E_r and H also increase with increasing concentration of Mn/Ca, but in a non-linear way. While very low levels of Mn/Ca are associated with a softer matrix at the base, higher Mn/Ca concentration is correlated with higher mechanical properties, but a further increase of the concentration does not change the mechanical performance substantially. This may point towards a threshold effect which could be related to the conflicting findings in the literature: while some authors found an enhancement of mechanical properties upon Mn incorporation [10, 14], others

did not [20]. There remains the question, why higher levels of Mn and Ca are present in the tip region, even though no further enhancement of *H* and *E*r was found. We speculate that they could serve a mechanical functionality that was not measured here, such as for example fracture toughness. Regarding the dimensions of both PS and NS, the tip diameter of NS is greater than PS. It has been demonstrated that small diameter tools are more likely to fracture during puncturing as the energy needed to cause a fracture is almost the same as the energy required to penetrate the target [37]. Therefore, in the case of PS, we can only speculate an adaptation of the epicuticle to be less susceptible to fracture may be paramount, since the *C. platnicki* scorpion uses its stinger much more frequently than *N. whitei* scorpions.

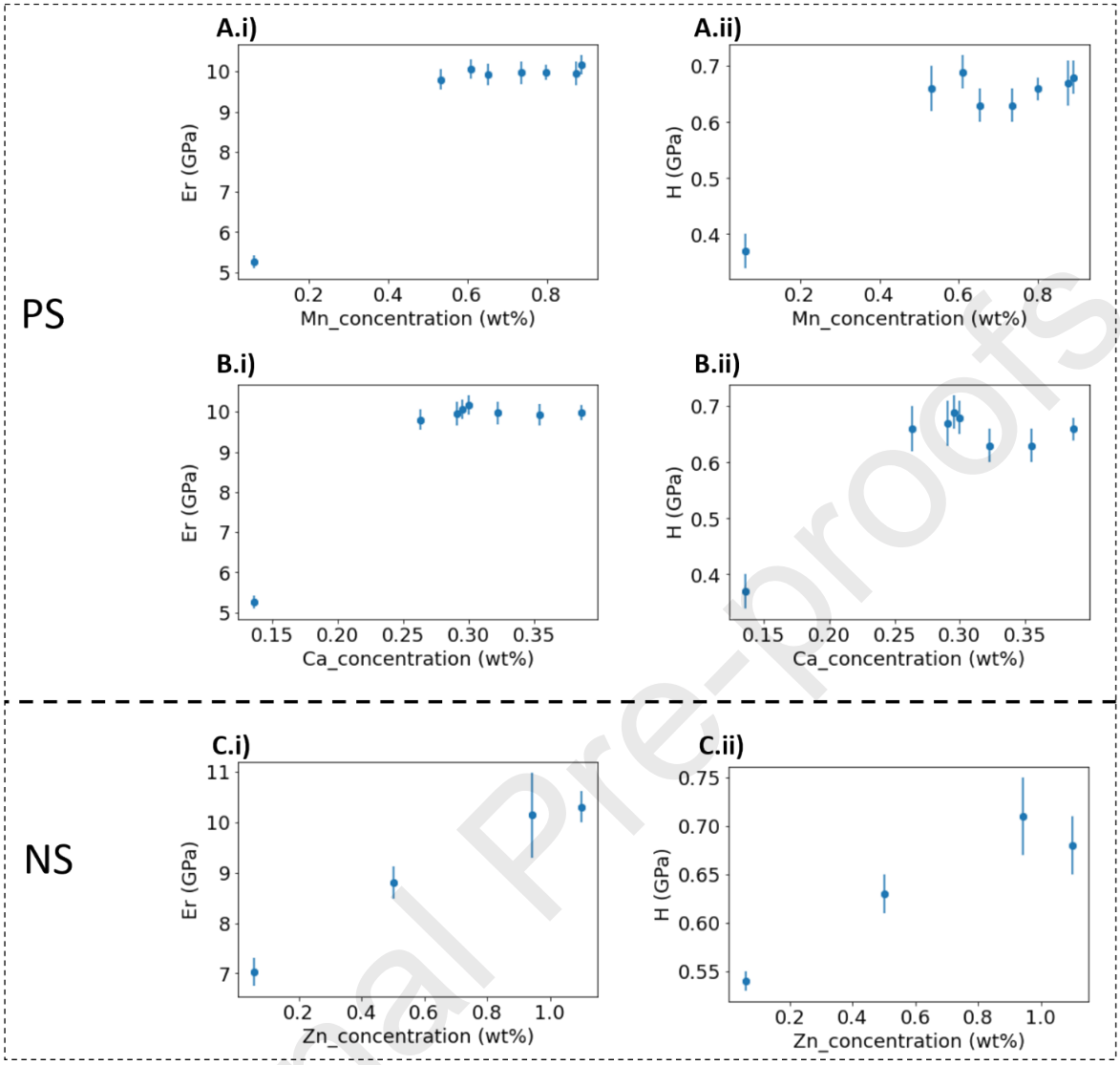

Figure 7: Evolution of the reduced elastic modulus in function of A.i) Mn, B.i) Ca concentration in PS and C.i) Zn concentration in NS and hardness in function of A.ii) Mn, B.ii) Ca concentration in PS and C.ii) Zn concentration in NS.

Furthermore, it should be noted that the epicuticle, although being the most exposed layer, is not the only load bearing part of scorpion stingers. As has been shown in the literature, the chitin fibre-rich exocuticle and endocuticle also play an important role. We found a higher degree of crystallinity of the chitin crystals in the concave region and at the base of the PS, where tensile and torsion stresses are expected. In NS the degree of crystallinity of the chitin crystals is lower than

PS at the base area. It is possible that also these differences are related to the different lifestyle, in particular the fact that *Nebo* scorpions do not use their stingers often to catch prey.

While the results presented in this study provide useful insights into the composition and structure of the scorpion stingers, it is important to recognize that biological systems, including scorpions, may exhibit variability across individuals within a species. Factors such as age, sex, and environmental conditions can contribute to this heterogeneity. Consequently, the measurements obtained for each species might not fully capture the range of possible variation across individual scorpions.

To enhance the generalisability of the findings, further studies could involve analysing a larger and more diverse set of samples from multiple individuals within each species. This would help to better understand the extent of variability and allow for a more comprehensive interpretation of how metal ion incorporation might differ within populations. Additionally, investigating environmental factors that influence the metal composition could provide insights into the biological processes underlying these patterns.

This first attempt in comparing the role of metal ions in the adaptation of specific mechanical functions in the stingers from different scorpion species with different lifestyle shows great promise. Conducting direct fracture measurements and *in situ* testing of the stinging action of both scorpions as well as studying the venom of the *C. platnicki* scorpion post stinging would allow a better understanding of the mechanical role of Mn/Ca in the epicuticle and the biological role of Zn in the venom canal.

V. Conclusion:

We showed the role of the chitin arrangement and elemental composition in enhancing the mechanical properties of scorpion stinger. We find that the arrangement and the degree of crystallinity and organisation of the chitin fibrils might be seen as an adaptation of the stinger to resist bending and twisting stresses. In addition, we compared the role of different metal ions incorporation in two types of scorpion stingers. We found that distinct type of scorpions uses different elemental distribution in their stinger. We showed that the incorporation of Zn is not always related to hardening purposes. We also showed that an increase of the Mn/Ca concentration is correlated with a substantial increase of mechanical properties, but a further increase of the concentration does not change the mechanical performance substantially. Our results shed new light on the formation of hard biological materials and possible biomechanical adaptations.

Acknowledgments:

We thank Karolina Peter and Leon Ploszczanski (Institute of Physics and Materials Science, BOKU University, Vienna, Austria) for their help with sample preparation and the SEM measurements. We acknowledge the European Synchrotron Radiation Facility (ESRF) for provision of beam time at BM05 and ID13 under proposal numbers MA-5735 (https://doi.esrf.fr/10.15151/ESRF-ES-1196501221) and IH-MA-299 (https://doi.esrf.fr/10.15151/ESRF-ES-934867651) and we would like to thank Aleksey Melnikov for assistance. We also thank Remi Tucoulou (ESRF) for providing the AXO reference sample and helping with the XRF calibration.

References:

[1] G. Fraenkel, K.M. Rudall, W.T. Astbury, The structure of insect cuticles, Proceedings of the Royal Society of London. Series B - Biological Sciences 134(874) (1947) 111-143.
[2] J. Blackwell, M.A. Weih, Structure of chitin-protein complexes: Ovipositor of the ichneumon fly Megarhyssa, J. Mol. Biol. 137(1) (1980) 49-60.
[3] J.F.V. Vincent, Arthropod cuticle: a natural composite shell system, Composites Part A: Applied Science and Manufacturing 33(10) (2002) 1311-1315.
[4] J.F.V. Vincent, U.G.K. Wegst, Design and mechanical properties of insect cuticle, Arthropod Struct. Dev. 33(3) (2004) 187-199.
[5] M. Erko, M.A. Hartmann, I. Zlotnikov, C. Valverde Serrano, P. Fratzl, Y. Politi, Structural and mechanical properties of the arthropod cuticle: Comparison between the fang of the spider Cupiennius salei and the carapace of American lobster Homarus americanus, J. Struct. Biol. 183(2) (2013) 172-179.
[6] M. Erko, O. Younes-Metzler, A. Rack, P. Zaslansky, S.L. Young, G. Milliron, M. Chyasnavichyus, F.G. Barth, P. Fratzl, V. Tsukruk, I. Zlotnikov, Y. Politi, Micro- and nano-structural details of a spider's filter for substrate vibrations: relevance for low-frequency signal transmission, J. R. Soc. Interface 12(104) (2015).
[7] C.F. Schaber, S. Flenner, A. Glisovic, I. Krasnov, M. Rosenthal, H. Stieglitz, C. Krywka, M. Burghammer, M. Müller, S.N. Gorb, Hierarchical architecture of spider attachment setae reconstructed from scanning nanofocus X-ray diffraction data, J. R. Soc. Interface 16(150) (2019) 20180692.
[8] Y. Politi, B. Bar-On, H.-O. Fabritius, Mechanics of Arthropod Cuticle-Versatility by Structural and Compositional Variation, in: Y. Estrin, Y. Bréchet, J. Dunlop, P. Fratzl (Eds.), Architectured Materials in Nature and Engineering: Archimats, Springer International Publishing, Cham, 2019, pp. 287-327.
[9] R. Schofield, H. Lefevre, M. Shaffer, Complementary microanalysis of Zn, Mn and Fe in the chelicera of spiders and scorpions using scanning MeV-ion and electron microprobes, Nuclear Instruments and Methods in Physics Research Section B: Beam Interactions with Materials and Atoms 40-41 (1989) 698-701.
[10] R.M.S. Schofield, J. Bailey, J.J. Coon, A. Devaraj, R.W. Garrett, M.S. Goggans, M.G. Hebner, B.S. Lee, D. Lee, N. Lovern, S. Ober-Singleton, N. Saephan, V.R. Seagal, D.M. Silver, H.E. Som, J. Twitchell, X. Wang, J.S. Zima, M.H. Nesson, The homogenous alternative to biomineralization: Zn- and Mn-rich materials enable sharp organismal “tools” that reduce force requirements, Scientific Reports 11(1) (2021) 17481.
[11] R.M.S. Schofield, H.W. Lefevre, PIXE-STIM microtomography: Zinc and manganese concentrations in a scorpion stinger, Nuclear Instruments and Methods in Physics Research Section B: Beam Interactions with Materials and Atoms 72(1) (1992) 104-110.
[12] H.C. Lichtenegger, T. Schöberl, J.T. Ruokolainen, J.O. Cross, S.M. Heald, H. Birkedal, J.H. Waite, G.D. Stucky, Zinc and mechanical prowess in the jaws of Nereis, a marine worm, Proc. Natl. Acad. Sci. U. S. A. 100(16) (2003) 9144-9149.
[13] R.M.S. Schofield, M.H. Nesson, K.A. Richardson, P. Wyeth, Zinc is incorporated into cuticular "tools" after ecdysis: The time course of the zinc distribution in "tools" and whole bodies of an ant and a scorpion, Journal of Insect Physiology 49(1) (2003) 31-44.
[14] M. Tadayon, O. Younes-Metzler, Y. Shelef, P. Zaslansky, A. Rechels, A. Berner, E. Zolotoyabko, F.G. Barth, P. Fratzl, B. Bar-On, Y. Politi, Adaptations for Wear Resistance and Damage Resilience: Micromechanics of Spider Cuticular “Tools”, Advanced Functional Materials 30(32) (2020) 2000400.
[15] Y. Politi, M. Priewasser, E. Pippel, P. Zaslansky, J. Hartmann, S. Siegel, C. Li, F.G. Barth, P. Fratzl, A Spider's Fang: How to Design an Injection Needle Using Chitin-Based Composite Material, Advanced Functional Materials 22(12) (2012) 2519-2528.
[16] C.C. Broomell, R.K. Khan, D.N. Moses, A. Miserez, M.G. Pontin, G.D. Stucky, F.W. Zok, J.H. Waite, Mineral minimization in nature's alternative teeth, J. R. Soc. Interface 4(12) (2007) 19-31.
[17] C.C. Broomell, M.A. Mattoni, F.W. Zok, J.H. Waite, Critical role of zinc in hardening of Nereis jaws, J. Exp. Biol. 209(16) (2006) 3219-3225.

[18] T.D. Morgan, P. Baker, K.J. Kramer, H.H. Basibuyuk, D.L.J. Quicke, Metals in mandibles of stored product insects: do zinc and manganese enhance the ability of larvae to infest seeds?, J. Stored Prod. Res. 39(1) (2003) 65-75.
[19] H. Birkedal , R.K. Khan, N. Slack , C. Broomell, H.C. Lichtenegger , F. Zok, G.D. Stucky , J.H. Waite Halogenated Veneers: Protein Cross-Linking and Halogenation in the Jaws of Nereis, a Marine Polychaete Worm, Chembiochem 7(9) (2006) 1392-1399.
[20] B.W. Cribb, A. Stewart, H. Huang, R. Truss, B. Noller, R. Rasch, M.P. Zalucki, Insect mandibles—comparative mechanical properties and links with metal incorporation, Naturwissenschaften 95(1) (2008) 17-23.
[21] B.W. Cribb, A. Rathmell, R. Charters, R. Rasch, H. Huang, I.R. Tibbetts, Structure, composition and properties of naturally occurring non-calcified crustacean cuticle, Arthropod Struct. Dev. 38(3) (2009) 173-178.
[22] H.-O. Fabritius, E.S. Karsten, K. Balasundaram, S. Hild, K. Huemer, D. Raabe, Correlation of structure, composition and local mechanical properties in the dorsal carapace of the edible crab Cancer pagurus, Zeitschrift für Kristallographie - Crystalline Materials 227(11) (2012) 766-776.
[23] D. Quicke, J. Palmer-Wilson, A. Burrough, G. Broad, Discovery of calcium enrichment in cutting teeth of parasitic wasp ovipositors (Hymenoptera: Ichneumonoidea), African Entomology 12 (2004) 259-264.
[24] G.A. Polis, The Biology of Scorpions, Stanford University Press1990.
[25] J. Kieffer, G. Ashiotis, PyFAI: a Python library for high performance azimuthal integration on GPU, (2014).
[26] V.A. Solé, E. Papillon, M. Cotte, P. Walter, J. Susini, A multiplatform code for the analysis of energy-dispersive X-ray fluorescence spectra, Spectrochimica Acta Part B: Atomic Spectroscopy 62(1) (2007) 63-68.
[27] P. Sudharshan Phani, W.C. Oliver, A critical assessment of the effect of indentation spacing on the measurement of hardness and modulus using instrumented indentation testing, Mater. Des. 164 (2019) 107563.
[28] W.C. Oliver, G.M. Pharr, An Improved Technique for Determining Hardness and Elastic- Modulus Using Load and Displacement Sensing Indentation Experiments, J. Mater. Res. 7(6) (1992) 1564-1583.
[29] Y. Bouligand, Twisted fibrous arrangements in biological materials and cholesteric mesophases, Tissue and Cell 4(2) (1972) 189-217.
[30] B. Bar-On, F.G. Barth, P. Fratzl, Y. Politi, Multiscale structural gradients enhance the biomechanical functionality of the spider fang, Nature Communications 5(1) (2014) 3894.
[31] H. Zhang, I. Kellersztein, G. Freychet, M. Zhernenkov, H. Daniel Wagner, J.R. Greer, Chemo-mechanical-microstructural coupling in the tarsus exoskeleton of the scorpion Scorpio palmatus, Acta Biomater 160 (2023) 176-186.
[32] I. Kellersztein, S.R. Cohen, B. Bar-On, H.D. Wagner, The exoskeleton of scorpions' pincers: Structure and micro-mechanical properties, Acta Biomater. 94 (2019) 565-573.
[33] Y. Politi, E. Pippel, A.C. Licuco-Massouh, L. Bertinetti, H. Blumtritt, F.G. Barth, P. Fratzl, Nano-channels in the spider fang for the transport of Zn ions to cross-link His-rich proteins pre-deposited in the cuticle matrix, Arthropod Struct Dev 46(1) (2017) 30-38.
[34] H.C. Lichtenegger, T. Schöberl, M.H. Bartl, H. Waite, G.D. Stucky, Response to comment on "High abrasion resistance with sparse mineralization: Copper biomineral in worm jaws", Science 301(5636) (2003).
[35] E. Ortiz, M. Rendón-Anaya, S.C. Rego, E.F. Schwartz, L.D. Possani, Antarease-like Zn-metalloproteases are ubiquitous in the venom of different scorpion genera, Biochimica et biophysica acta 1840(6) (2014) 1738-46.

[36] S. Khan, M. Lang, A Comprehensive Review on the Roles of Metals Mediating Insect–Microbial Pathogen Interactions, Metabolites, 2023.
[37] R.M.S. Schofield, S. Choi, J.J. Coon, M.S. Goggans, T.F. Kreisman, D.M. Silver, M.H. Nesson, Is fracture a bigger problem for smaller animals? Force and fracture scaling for a simple model of cutting, puncture and crushing, Interface Focus 6(3) (2016) 20160002.

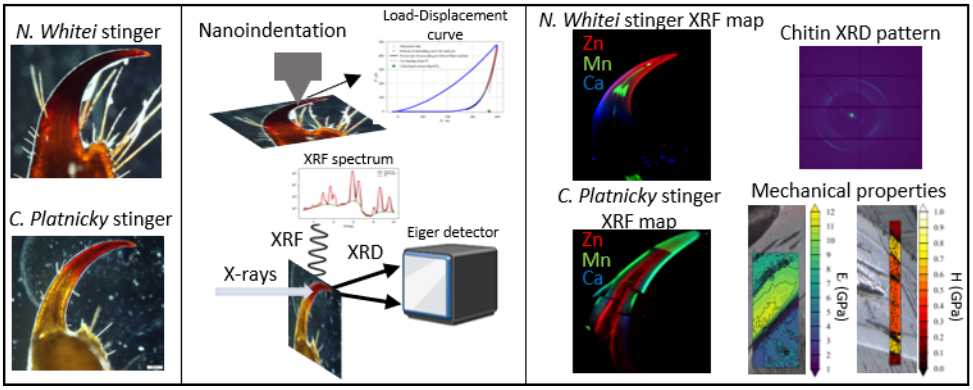

Declaration of interests

☒ The authors declare that they have no known competing financial interests or personal relationships that could have appeared to influence the work reported in this paper.

☐ The authors declare the following financial interests/personal relationships which may be considered as potential competing interests: